The influence of the methionine residue on the dissociation mechanisms of photoionized methionine-enkephalin probed by VUV action spectroscopy

Simon Dörner, Lucas Schwob, Kaja Schubert, Marion Girod, Luke Macaleese, Cornelius Pieterse, Thomas Schlathölter, Simone Techert, Sadia Bari

Eur. Phys. J. D (2021) 75:142
https://doi.org/10.1140/epjd/s10053-021-00147-y

THE EUROPEAN PHYSICAL JOURNAL D

Regular Article – Atomic and Molecular Collisions

The influence of the methionine residue on the dissociation mechanisms of photoionized methionine-enkephalin probed by VUV action spectroscopy

Simon Dörner[1,a], Lucas Schwob[1], Kaja Schubert[1], Marion Girod[2], Luke MacAleese[3], Cornelius L. Pieterse[4], Thomas Schlathölter[5], Simone Techert[1,6], and Sadia Bari[1,b]

[1] Deutsches Elektronen-Synchrotron DESY, Notkestrasse 85, 22607 Hamburg, Germany
[2] Univ Lyon, Université Claude Bernard Lyon 1, Institut des Sciences Analytiques, CNRS UMR 5280, 5 rue de la Doua, 69100 Villeurbanne, France
[3] Univ Lyon, Université Claude Bernard Lyon 1, Institut Lumière Matière, CNRS UMR 5306, 69622 Lyon, France
[4] National Physical Laboratory, Hampton Road, Teddington TW11 0LW, UK
[5] Zernike Institute for Advanced Materials, University of Groningen, Nijenborgh 4, 9747 AG, Groningen, The Netherlands
[6] Institut für Röntgenphysik, Georg-August Universität Göttingen, Friedrich-Hund-Platz 1, 37077 Göttingen, Germany

Received 31 January 2021 / Accepted 7 April 2021 / Published online 27 April 2021

Abstract. VUV action spectroscopy has recently gained interest for the study of peptides and proteins. However, numerous aspects of the fundamental processes involved in the photodissociation are yet to be understood. It can, for example, be expected that sulfur-containing amino-acid residues have a significant impact on the dissociation processes following photoionization because of their potential involvement in the transport of electron holes in proteins. In order to investigate the influence of the sulfur-containing methionine residue on the VUV photodissociation of a small peptide a VUV action spectroscopy study of gas-phase protonated methionine-enkephalin and leucine-enkephalin in the photon energy range of 6–35 eV was performed. The results show that upon non-ionizing photoexcitation, the fragmentation patterns of the two peptides are nearly identical, whereas significant differences were observed upon photoionization. The differences between the fragment yields and the identified specific dissociation channels for methionine-enkephalin could be explained by the high electron hole affinity of sulfur, which efficiently directs the radical to the methionine side chain. Additionally, for both peptides the presence of the intact photoionized precursor ions was confirmed by their isotopic patterns and the stability of these species could be evaluated.

1 Introduction

The pioneering experiments on the synchrotron-based vacuum ultraviolet (VUV) action spectroscopy of gas-phase protonated peptides and proteins were carried out ten years ago [1,2]. These experiments have only been made possible thanks to the high brilliance of 3rd generation synchrotrons and the use of state-of-the-art tandem mass spectrometers in combination with electrospray ionization (ESI) sources, enabling delivery of such fragile systems into the gas phase. In the frame of radiation damage, VUV photons offer a unique opportunity for understanding, at the molecular level, the fundamental physical processes following ionization. Moreover, the recent advances in intense tabletop VUV gas-discharge lamp sources have attracted increasing interest over the past years for the utilization of VUV light in mass spectrometry as a new tool for protein sequencing [3,4]. Today, while the popularity of this technique is growing, data on peptides and proteins are scarce (since carrying such experiments remains challenging) and fundamental photon-induced processes in play are yet to be understood.

Action spectroscopy in the VUV range, commonly with photon energies ranging from 5 to 40 eV, enables, with increasing photon energy, probing of photoexcitations and photoionizations from outer down to inner valence levels. Typically, the ionization energy (IE) of a singly protonated peptide is around 10 eV [5] and increases by ∼1 eV/charge with the protonation state because of the increasing Coulombic attraction between the departing electron and the positive charges of the protons [6]. However, the stability of a protonated peptide towards ionization is largely dependent on its size and on its ability to unfold its structure to compensate the instability caused by the increased Coulombic repulsion. In a systematic investigation of the influence of the peptide length, it has been shown that non-

[a] e-mail: simon.doerner@desy.de (corresponding author)
[b] e-mail: sadia.bari@desy.de (co-corresponding author)

dissociative ionization may only be observed for peptides with masses higher than 900 Da [7]. Above the IE, ionization in deeper valence orbitals becomes favorable. The electronic energy may be quickly converted into vibrational energy by intramolecular vibrational energy redistribution (IVR), leading, in most cases, to statistical fragmentation. While large systems, such as proteins, can withstand the increased charge and stay intact following ionization by distributing the internal energy over their many degrees of freedom, smaller peptides undergo extensive fragmentation into small internal fragments, immonium ions and side-chain fragments [8].

Photoionization is characterized by the valence hole in the radical species $[M+nH]^{(n+1)+\bullet}$ caused by the electron removal. In competition with proton-directed and proton-remote dissociation processes characteristic for vibrationally excited protonated peptides [9], radical cations undergo very specific radical-induced dissociation (RID) pathways, leading, for example, to efficient side-chain losses [4,10] while retaining some non-covalent complexes intact [11,12]. Common RID techniques based on electron transfer or electron capture involve charge reduction of protonated species and can, consequently, only be applied to multiply charged systems. As photoionization leads to a charge increase, VUV-activation does not have this restriction and is, therefore, an advantageous tool for probing these radical-driven processes on singly charged species. Still, more knowledge is required for the interpretation of the photodissociation and dissociative photoionization spectra of peptides and proteins and for the understanding of the underlying mechanisms leading to the observed fragmentation pathways.

In this paper, we want to investigate the influence of a sulfur-containing residue on specific bond cleavage in a peptide upon VUV photoabsorption. These amino acids, namely cysteine and methionine, are known for participating in electron transfer reactions within proteins thanks to their low ionization potentials and their ability to interact with aromatic side chains [13–15]. Because sulfur-containing residues can capture and transiently carry electron holes they are likely to influence the fragmentation pathways of photoionized protonated peptides. In the present article we report an experimental investigation of the protonated pentapeptides leucine-enkephalin (LeuEnk, Tyr-Gly-Gly-Phe-Leu) and its sulfur-containing pendant methionine-enkephalin (MetEnk, Tyr-Gly-Gly-Phe-Met) by VUV action spectroscopy. LeuEnk, which has become a mass spectrometry standard [16], has been studied intensively by various activation methods, including VUV radiation [1,17,18], and we have recently reported an X-ray action spectroscopy study of protonated MetEnk at the sulfur L-edge [19]. Our experimental results demonstrate a characteristic influence of the methionine residue on the fragmentation pathways following photoexcitation and photoionization of MetEnk and also complement the existing results on LeuEnk. First, we present the photodissociation mass spectra of both peptides measured below and above the IE and explain the characteristic differences between the fragmentation patterns. Then, we discuss the influence of the methionine residue on the dissociation mechanisms of MetEnk based on the experimental partial ion yield spectra of several photoproducts and the comparison with collision-induced dissociation results.

2 Experimental section

2.1 VUV action spectroscopy

The VUV action spectroscopy experiments were carried out at the U125-2_NIM beamline [20,21] of the BESSY II synchrotron (Helmholtz-Zentrum Berlin) using photon energies ranging from 6 to 35 eV. The photon energy bandwidth ΔE_{ph} at this beamline follows an $(E_{ph})^2$ trend, typical for spherical grating monochromators, which can be approximated by the following empirical equation:

$$\Delta E_{ph} = (3 \times 10^{-5}\,\mathrm{eV^{-1}mm^{-1}} \times E_{ph}^2 + 2 \times 10^{-6}\,\mathrm{mm^{-1}} \times E_{ph}) \times S_w \quad (1)$$

where S_w is the opening width of the beamline slits in mm. In order to keep the photon energy bandwidth below 100 meV and constant over the measurement range, the slits where opened from 300 μm at 25.5 eV and above, to up to 1800 μm for photon energies of 14.5 eV and below.

For the photon energies below 11 eV, an MgF_2 window was inserted into the beamline to filter out high harmonic photons. Above 11 eV the MgF_2 filter could not be used because of a highly decreased photon transmission efficiency. Therefore, the mass spectra measured in the energy range of 11 to 12.5 eV still showed distinguishable signs of photodissociation processes induced by absorption of second harmonic photons. In order to avoid a misinterpretation of these spectra they are not shown in the following. Above 12.5 eV, the contribution of high harmonic photons was negligible.

A home-built tandem mass spectrometer, described in detail elsewhere [22], was coupled to the beamline in order to record the VUV action spectra for the studied peptides. An ESI source, operated here in positive ion mode, was used to transfer protonated peptides into the gas phase. The ions enter a heated capillary and are focused by an ion funnel before passing a radio-frequency octupole. Precursor ions of interest are then mass-to-charge selected in a quadrupole mass filter and injected into a 3D ion Paul trap (low-mass cutoff $m/z < 75$). In the trap the ions are accumulated while being kinetically cooled in helium buffer gas at room temperature. The helium buffer gas is pulsed synchronously to the precursor ions (50–100 ms) and is pumped down before the precursor ions are irradiated with VUV light. The exposure time, typically several hundreds of milliseconds, is controlled by an electrome-

chanical beam shutter. The photon flux is recorded with a calibrated photodiode placed downstream of the ion trap. The irradiation time is adjusted to the photon flux and precursor ion yield such that upon irradiation a relative depletion of the precursor ion peak of $< 10\%$ is achieved. Consequently, when considering the consecutive absorption of two photons as independent processes, statistically, $< 10\%$ of the photoproducts are attributed to double photon absorption. Cation products are extracted from the trap into a reflectron time-of-flight mass spectrometer to record the interaction mass spectra as a function of the photon energy. The experimental mass resolution of about $m/\Delta m = 2200$ is high enough to allow for the separation of isotopic peaks of doubly charged ions in the studied mass range.

During the experiment, per acquisition cycle one precursor-only spectrum (no photon beam) and two interaction spectra were recorded and at every photon energy the obtained data were averaged over 75–100 acquisition cycles. This way, the effects of long time-scale fluctuations inherent to the setup (ESI source, trapping efficiency) on the averaged spectra were minimized. The area of the precursor ion main peak in a precursor-only spectrum was used as a measure for the yield of precursor ions in the trap. In order to correct the data for fragments arising from collisional fragmentation of the precursor ions, the averaged precursor-only spectra were subtracted from the respective averaged interaction mass spectra. The corrected interaction spectra were then normalized to the photon flux, exposure time and precursor ion yield. Thus, the area of a mass peak in a normalized interaction spectrum represents the fragment yield, in arbitrary units, per photon and precursor ion.

2.2 Collision-induced dissociation

The collision-induced dissociation (CID) experiments were performed on a hybrid quadrupole-Orbitrap Q-Exactive® mass spectrometer (Thermo Fisher Scientific, San Jose, CA, USA) equipped with a HESI (heated ESI) source. The source was operated in positive ion mode with an ion spray voltage of 4500 V. The sheath gas and auxiliary gas (nitrogen) flow rates were set at 20 and 15 (arbitrary unit), respectively, with a HESI vaporizer temperature of 250 °C. The ion transfer capillary temperature was 250 °C. The S-lens radio frequency was set at 55 (arbitrary unit). The Orbitrap resolution was $m/\Delta m = 140,000$. The Automatic Gain Control (AGC) target was 5×10^6 and the maximum injection time was set to 100 ms. The CID experiments were performed with 10 ms activation time, in N_2 and at a collision energy in the laboratory frame of 25 eV, resulting in center-of-mass energies of 1.20 and 1.16 eV for LeuEnk and MetEnk, respectively. A window of 3.0 m/z was applied for precursor isolation. The peptides were electrosprayed at a flow rate of 5 μL/min.

2.3 Sample preparation

For both the VUV and CID experiment, the samples were prepared in the same way. Leucine-enkephalin (Tyr-Gly-Gly-Phe-Leu; 555 u) acetate salt hydrate (purity $\geq$ 95%), [Met^5]-enkephalin (Tyr-Gly-Gly-Phe-Met; 573 u) acetate salt hydrate (purity $\geq$95%), methanol, water and formic acid were purchased from Merck/Sigma-Aldrich and were used without additional purification. The sample solutions were prepared at 30 μM concentration in 1:1 water/methanol with 1 vol% of formic acid for protonation of the peptides.

3 Results and discussion

3.1 Total ion yields

The depletion of the precursor ion peak was determined by subtracting the precursor ion yield in the interaction spectrum from the precursor ion yield in the respective precursor-only spectrum. The normalized precursor ion depletion as a function of the photon energy for both peptides is shown in Fig. 1a. At low photon energies (< 10.75 eV), because of the low photon flux, the precursor ion depletion values measured are very small and, thus, more prone to fluctuations. However, at higher photon energy (> 13 eV), the depletion curves show more similarity between both peptides, characterized by an, on average, 13% higher depletion for LeuEnk.

The total ion yields were calculated for both peptides by summing up the areas of all detected fragments in an interaction spectrum. The photon-energy dependent total ion yield spectra of both peptides (Fig. 1b) show two weak features A and B at ~7 eV and ~10 eV, respectively, an intense main feature C ranging from

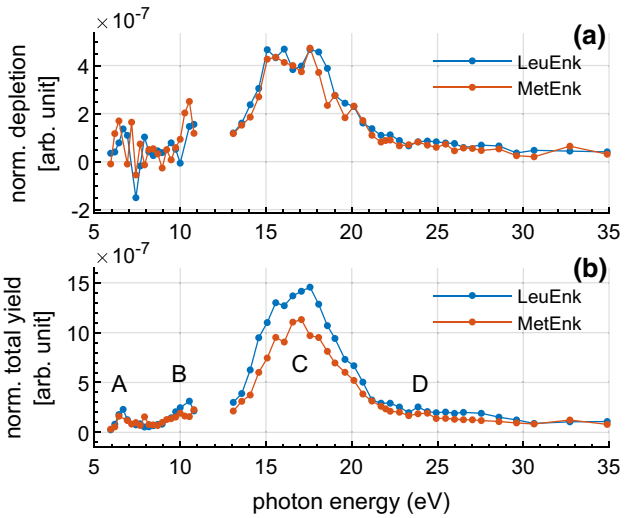

Fig. 1 Normalized **a** precursor ion depletion and **b** total ion yield measured for protonated LeuEnk and MetEnk

14 to 21 eV and a broad, weak feature D in the photon energy range of 21–31 eV. Features A and B are also clearly visible in the ion yield spectra measured by Ranković et al. [17].

Based on the photoelectron data of individual amino acids reported by Cannington et al. [23] the vertical ionization potentials of LeuEnk and MetEnk should be 9.2 eV (π orbitals of the phenylalanine side chain) and 8.7 eV (n_S orbital of the methionine side chain), respectively. In a series of computational studies on amino acids and polypeptides by Serrano-Andrés et al. [24] several types of photoexcitations have been identified: transitions from the σ orbitals of oxygen lone-pair electrons to the amide π^* orbital (W bands) at ∼5.5 eV, $\pi \rightarrow \pi^*$ transitions within a peptide bond (NV bands) at ∼6.5 eV as well as charge transfer transitions from a peptide bond π orbital to π^* orbitals of neighboring peptide bonds (CT bands) in the photon energy range of around 7–9.5 eV. Furthermore, photoexcitations within the aromatic carbon rings of phenylalanine and tyrosine can be expected at ∼7 eV [25].

Based on this information, we attribute feature A to photoexcitations in the aromatic side chains of phenylalanine and tyrosine as well as within peptide bonds. Peak B is caused by charge transfer transitions or by photoionizations from the highest occupied molecular orbitals (HOMOs). The main feature C is based mainly on direct photoionizations from outer valence orbitals, with contributions from photoexcitations of inner valence electrons. Feature D can be attributed to photoionizations from inner valence orbitals.

In the normalized total ion yield spectra of the two peptides (Fig. 1b) there is a clear difference between the intensities of feature C, which is around 30% higher for LeuEnk than for MetEnk. Since this value exceeds the relative difference between the precursor ion depletions measured for LeuEnk and MetEnk it cannot be explained based on the photoabsorption cross sections of the molecules. The most probable explanation for this effect is that there is a large abundance of fragments of MetEnk with mass-to-charge ratios below the trapping window cut-off, *e.g.* charged partial fragments of the methionine side chain.

3.2 Fragment identification

The mass spectra measured at photon energies of 6.4, 10.8 and 16.5 eV are shown in Fig. 2 together with the mass spectrum resulting from CID at 25 eV collision energy. The photon energies represent the regimes dominated by low-energy photoexcitation (feature A), high-energy photoexcitation (feature B) and photoionization (feature C), respectively (see Sect. 3.1). The chemical structure of MetEnk and the cleavage sites of different observed fragments are shown in Fig. 3. A selection of detected peaks (Table 1) is discussed in the following.

Fragments produced by cleavage of the peptide backbone are labeled according to the nomenclature established by Roepstorff and J. Fohlman [26]. For immonium ions (single-residue fragments formed by a combination of a-type and y-type cleavage) and full side-chain fragments the abbreviations X_{im} and X_{sc} are being used, where X is the one-letter code of an amino acid.

3.2.1 Photoexcitation at 6.4 eV

The mass spectra measured upon photoexcitation at 6.4 eV are shown in Fig. 2b. Overall, the high-mass region (above *m/z* 150) of the mass spectrum of LeuEnk is in good agreement with the spectrum measured at 6.7 eV by Ranković et al. [17]. The most intense peak for both peptides is the a_4 fragment at *m/z* 397. Other prominent peaks observed for both systems are the phenylalanine immonium ion (F_{im}) at *m/z* 120, the b_3 fragment at *m/z* 278 as well as the internal y_3b_4 and y_2b_4 fragments at *m/z* 205 and 262, respectively. Peaks measured at *m/z* 279 for LeuEnk and at *m/z* 297 for MetEnk are due to y_2 fragments. An intense peak at *m/z* 150 observed for MetEnk is attributed to the y_1 fragment. The LeuEnk spectrum exhibits a corresponding weak peak at *m/z* 132. For both peptides a weak peak attributed to the tyrosine immonium ion (Y_{im}) was detected at *m/z* 136. Additionally, a trace of the methionine immonium ion (M_{im}) of MetEnk was detected at *m/z* 104, while the leucine immonium ion (L_{im}), expected at *m/z* 86, was entirely absent in the spectrum of LeuEnk. The mass spectra of both peptides show weak peaks at *m/z* 323 and 380. In a comprehensive MS^n CID study on LeuEnk it has been shown that these peaks correspond to a loss of 17 u and 17+57 u from a_4, attributed to the sequential loss of an NH_3 group ($a_4 - NH_3$) and a glycine residue ($a_4 - NH_3 - G$) [27]. All of the above mentioned fragments were also observed in the respective mass spectra obtained by low-energy CID (Fig. 2a), which shows that the fragmentation at 6.4 eV is largely driven by IVR.

Previously unreported peaks at *m/z* 499, 512 and 529 were measured for MetEnk only. These peaks were not observed upon CID of MetEnk (Fig. 2a). We attribute the first two peaks to neutral losses in the Met residue from the precursor ions, leading to the $[M+H - C_3H_7S^{\bullet}]^{+\bullet}$ and $[M+H - C_2H_6S]^+$ fragments, respectively. Analogous peaks corresponding to neutral leucine side-chain losses from LeuEnk were not observed. Losses of these neutral methionine side chain fragments have been previously reported for VUV photodissociation of substance P [5]. The peak at *m/z* 529 is most likely due to neutral loss of the carboxylic acid group, leading to the $[M+H - COOH]^+$ fragment.

3.2.2 Photoexcitation at 10.8 eV

The mass spectra measured upon irradiation of the two peptides with 10.8 eV photons are shown in Fig. 2c. The yields of fragments b_3, y_2 and y_3b_4 of both peptides are strongly decreased compared to the yields measured at 6.4 eV. Furthermore, no fragments were detected at *m/z* ratios higher than 279, including a_4, the fragment with the highest yields measured at 6.4 eV. These observations are in contrast to the experimental data of

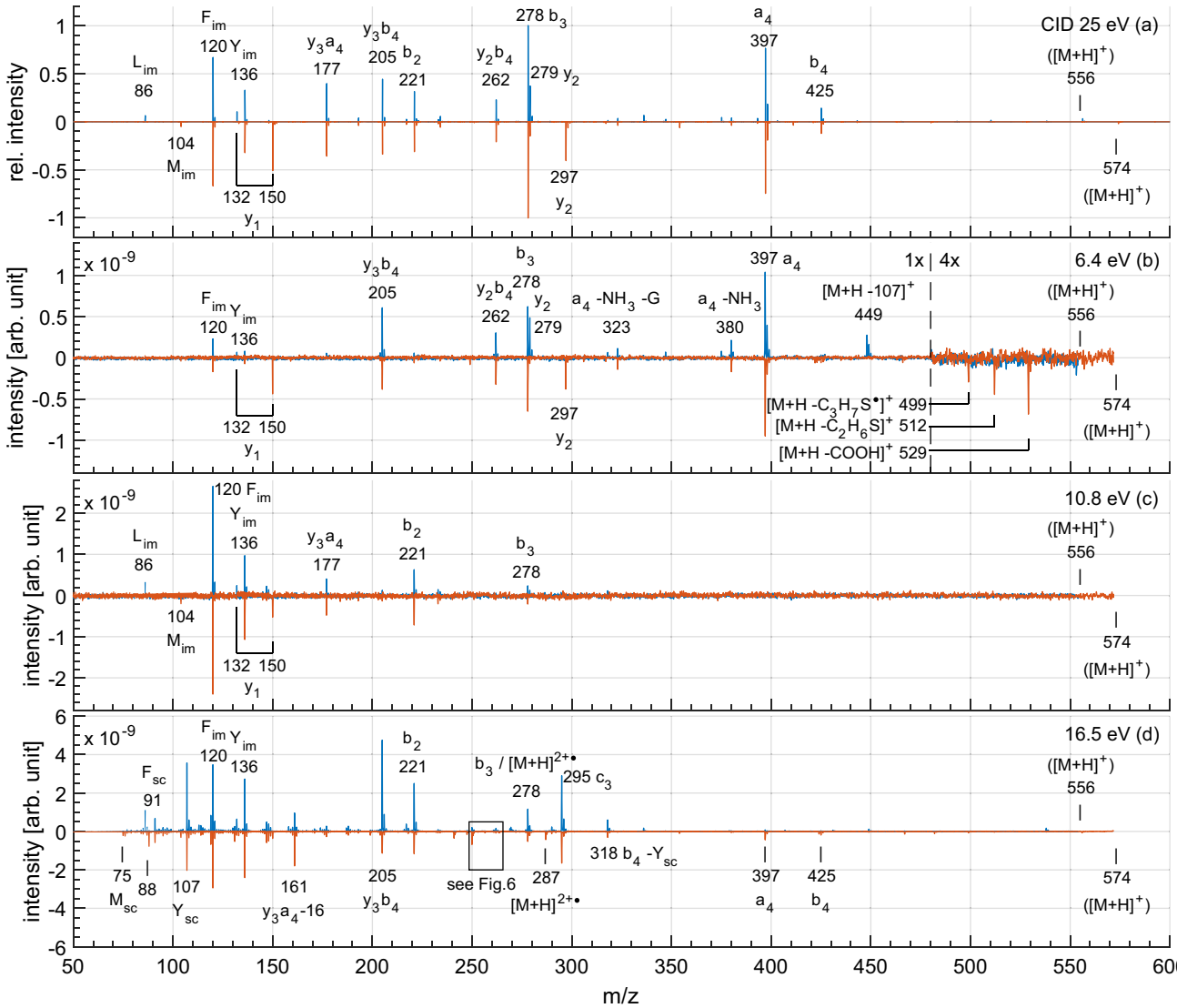

Fig. 2 Mass spectra of LeuEnk (blue) and MetEnk (red, inverted) obtained by **a** CID at 25 eV collision energy and photodissociation at photon energies of **b** 6.4, **c** 10.8 and **d** 16.5 eV. The photodissociation mass spectra are cut 2 *m/z* before the precursor ion peaks ($[M+H]^+$), as they would appear as negative peaks because of the data processing

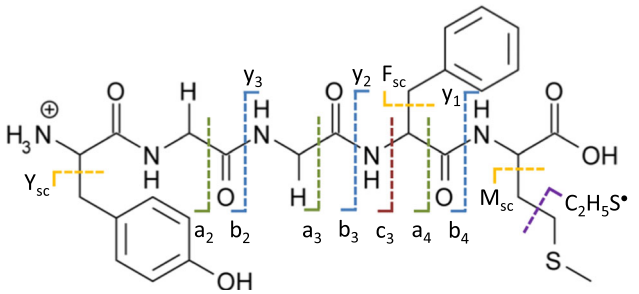

Fig. 3 Chemical structure of protonated MetEnk. The dotted lines indicate the cleavage sites of observed fragments

LeuEnk reported by Ranković et al. [17] where larger sequence fragments like a_4 and b_4 are still observed at 8.4 and 12.8 eV and the yields of b_3, y_2 and y_3b_4 (GF) are significantly higher. The reason for this discrepancy could be grounded in the fact that in the experiments carried out by Ranković et al. the helium buffer gas was present in the trap during the entire time while in our case it is pumped down before irradiation. This could have two consequences: (1) Photofragments with high kinetic energies may be lost in our instrument but be cooled down in the buffer gas and trapped in the other experiment. (2) When considering the possibility that the larger sequence fragments formed at these photon energies are in an excited, metastable state, collisions with the buffer gas would result in the stabilization of these fragments while, in our experiment, post-dissociation of the fragments would take place in the absence of collisional cooling. However, our extended mass axis in the low-mass range allows us to observe the strong increase of F_{im} and Y_{im} which, in fact, dominate

Table 1 Relative intensities and assignments of the peaks in the mass spectra measured upon irradiation of protonated LeuEnk and MetEnk with 6.4, 10.8 and 16.5 eV photons. The relative intensities are given in percent of the most intense signal in the respective mass spectrum

LeuEnk Rel. intensity in %						MetEnk	Rel. intensity in %			
16.5 eV	10.8 eV	6.4 eV	CID	*m/z*	Assignment	*m/z*	CID	6.4 eV	10.8 eV	16.5 eV
Precursor ions										
				556	$[M+H]^+$	574				
Singly charged species										
				511	$[M+H - COOH]^+$	529		16		
					$[M+H - C_2H_6S]^+$	512		11		
					$[M+H - C_3H_7S^\bullet]^{+\bullet}$	499		7		
2		29		449	$[M+H - Y_{sc}]^+$	467				
			14	425	b_4	425	12			4
		100	76	397	a_4	397	74	100		10
		19	4	380	$a_4 - NH_3$	380	4	21		
		12	4	323	$a_4 - NH_3 - G$	323	4	15		
11	4	6		318	$b_4 - Y_{sc}$	318				8
4	1	35	22	279	y_2	297	40	45		
54				295	c_3	295				41
8	8	67	100	278	b_3	278	100	79	8	14
3	2	34	23	262	y_2b_4	262	21	37	3	2
4				250	a_3	250				14
51	19	7	31	221	b_2	221	31	8	24	33
100	5	72	44	205	y_3b_4	205	34	53	7	32
6	11	67	40	177	y_3a_4	177	36	6	16	7
21				161	$y_3a_4 - 16$	161				55
14	8	9	10	132	y_1	150	50	65	17	11
11	8			147	y_2b_4	147			5	16
64	31	10	33	136	Y_{im}	136	32	9	43	79
83	100	38	67	120	F_{im}	120	67	28	100	100
89				107	Y_{sc}	107				69
					M_{im}	104	5	7	9	11
18				91	F_{sc}	91				21
				88	$C_3H_6NO_2^+$	88				27
					M_{sc}	75				7
29	12		6	86	L_{im}					
Doubly charged species										
15				278	$[M+H]^{2+\bullet}$	287				12
1				270	$[M+H - 16]^{2+\bullet}$	279				5
3				269.5	$[M+H - 17]^{2+\bullet}$	278.5				5
3				269	$[M+H - 18]^{2+\bullet}$	278				14
					$[M+H - CH_3S^\bullet]^{2+}$	263.5				2
					$[M+H - C_2H_5S^\bullet]^{2+}$	256.5				2
					$[M+H - C_3H_6S]^{2+\bullet}$	250				6

the fragmentation pathways. Additionally, we observe that the yield of M_{im} of MetEnk is slightly increased and L_{im} of LeuEnk appears at *m/z* 86.

Furthermore, the spectra of both peptides feature significant peaks at *m/z* 177 and 221. These signals are attributed to the y_3a_4 and b_2 ion, respectively. Overall, the yields of backbone fragments are reduced in favor of the production of immonium ions. All of these fragments were also observed upon CID (Fig. 2a). This shows that the fragmentation at 10.8 eV is still driven by IVR. However, compared to 6.4 eV, new dissociation channels are probed while others are quenched.

3.2.3 Photoionization at 16.5 eV

Figure 2c shows the mass spectra measured for the two peptides at 16.5 eV. Additionally, the low-mass region (*m/z* 70–110) of these spectra are shown in Fig. 4. The mass spectra of the two peptides show significant differences. Furthermore, the mass spectra differ greatly from those measured upon photoexcitation (Fig. 2b/c) and CID (Fig. 2a). It can, therefore, be assumed that at photon energies above the IE, mechanisms contribute to the dissociation of the two peptides that are fundamentally different from IVR and more dependent on the chemical structure of the amino-acid side chains.

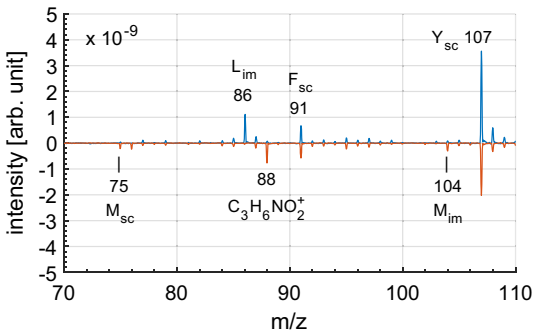

Fig. 4 Zoomed low-mass region of the mass spectra of LeuEnk (blue) and MetEnk (red, inverted) obtained by photodissociation at a photon energy of 16.5 eV (Fig. 2d)

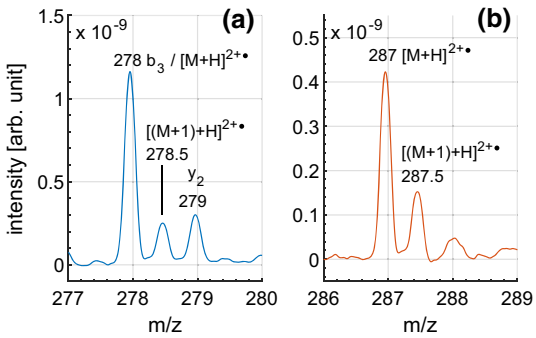

Fig. 5 Zoomed mass spectra of protonated **a** LeuEnk and **b** MetEnk obtained by photodissociation at a photon energy of 16.5 eV, covering the isotopic patterns of the photoionized precursor ions

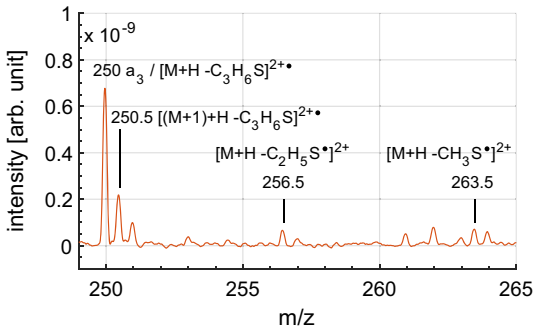

Fig. 6 Zoomed mass spectrum of protonated MetEnk obtained by photodissociation at a photon energy of 16.5 eV, covering the methionine side-chain losses from the photoionized precursor ion

For both peptides the most prominent peaks only appearing at 16.5 eV are the phenylalanine and tyrosine side-chain fragments (F_{sc} and Y_{sc}) at m/z 91 and 107 as well as fragments $y_3a_4 - 16$ and c_3 at m/z 161 and 295, respectively. The mass spectrum measured for MetEnk also features the methionine side-chain fragment M_{sc} at m/z 75. The corresponding leucine side-chain fragment of LeuEnk, expected at m/z 57, was not observed. However, we cannot conclude whether this fragment is produced or not as its mass is below the low-mass trapping cut-off. Additionally, a distinct peak at m/z 88 was detected for MetEnk. We attribute this peak to a C-terminal fragment with sum formula $C_3H_6NO_2^+$ (see Sect. 3.3.2).

The mass spectrum of MetEnk features a peak at m/z 287, corresponding to the photoionized precursor ion $[MetEnk+H]^{2+\bullet}$ (see isotopic pattern in Fig. 5b). The photoionized LeuEnk precursor ion $[LeuEnk+H]^{2+\bullet}$ was detected at m/z 278 (see isotopic pattern in Fig. 5a). The b_3 fragment of LeuEnk has a mass of 278 u as well. Previous studies [1,17] could not solve the ambiguity whether the peak at m/z 278 is due to the $[LeuEnk+H]^{2+\bullet}$ ion, the b_3 fragment or both species. However, the presence of the photoionized LeuEnk precursor ion is clearly confirmed by the isotopic peak detected at m/z 278.5. While it has been reported before that peptides with masses below 900 Da cannot assume a stable ground state upon photoionization [7], our present results clearly demonstrate that non-dissociative photoionization is possible, although less favored in comparison to photodissociation, in protonated peptides with masses as low as 556 u.

A clear peak at m/z 250 and weak peaks at m/z 256.5 and 263.5 (see Fig. 6) were detected for MetEnk. These peaks are in line with neutral losses of partial methionine side chains with sum formulas C_3H_6S (74 u), $C_2H_5S^\bullet$ (61 u) and $CH_3S^\bullet$ (47 u) from the photoionized precursor ion. Analogous fragments of substance P produced upon VUV photodissociation have been reported previously [5]. A weak peak at m/z 250 was also detected for LeuEnk. It is, therefore, likely that in the case of MetEnk this peak is both due to the a_3 and $[M+H-C_3H_6S]^{2+\bullet}$ fragments. Furthermore, weak peaks corresponding to neutral losses with masses 16 u ($NH_2^\bullet$), 17 u ($OH^\bullet/NH_3$) and 18 u (H_2O) from the photoionized precursor ion were observed for both peptides.

3.3 Partial ion yields

3.3.1 Photoionized precursor ions $[M+H]^{2+\bullet}$

In our experiment, photoionized precursor ions can only be produced by direct photoionization. Therefore, the appearance energies of the $[M+H]^{2+\bullet}$ ions of LeuEnk and MetEnk are direct measures for their IEs. The photon energy dependent normalized yields of the $[MetEnk+H]^{2+\bullet}$ ion (m/z 287) and of its isotopic peak, detected at m/z 287.5, are shown in Fig. 7a. The yields of the isotopic peak were divided by the ratios between the areas of the $[(M+1)+H]^+$ and $[M+H]^+$ precursor ion peak, measured in the respective precursor-only spectra. The ion yield spectra of both species are in high agreement. This confirms, that there are no fragments of MetEnk with an m/z ratio of 287 and the mass peak is exclusively due to the $[MetEnk+H]^{2+\bullet}$ ion.

As mentioned before, the $[LeuEnk+H]^{2+\bullet}$ ion and the b_3 fragment of LeuEnk both have an m/z ratio of 278 (see Fig. 5a). The photon energy dependent normalized yields of this peak and the corrected yields of

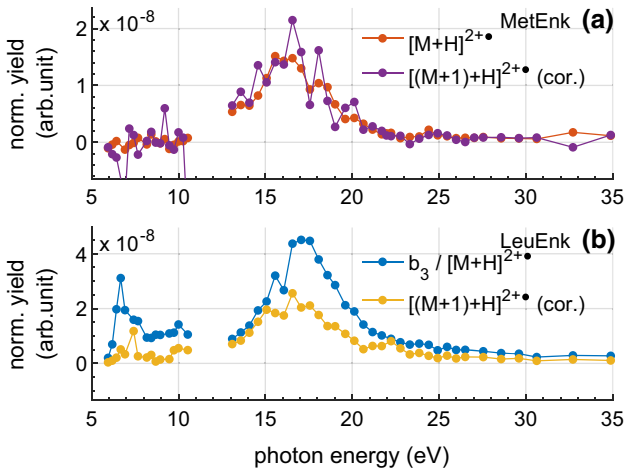

Fig. 7 Normalized yields of the photoionized precursor ions ($[M+H]^{2+\bullet}$) and their isotopic peaks ($[(M+1)+H]^{2+\bullet}$) of protonated **a** MetEnk and **b** LeuEnk measured upon VUV photoabsorption. The yields of the isotopic peaks are corrected by the ratios between the yields of the trapped precursor isotopes

the $[(LeuEnk+1)+H]^{2+\bullet}$ ion (m/z 278.5) are shown in Fig. 7b. When comparing these spectra to the yield spectrum of the b_3 fragment of MetEnk (see Fig. 8g) it becomes clear that all yield in the photoexcitation regime of the $b_3/[LeuEnk+H]^{2+\bullet}$ spectrum as well as roughly half of the yield on the right flank of feature C can be attributed to the b_3 fragment while the left flank of feature C appears to be solely due to the $[LeuEnk+H]^{2+\bullet}$ ion. Furthermore, the corrected yield of the isotopic peak is a solid representation for the actual yield of the photoionized precursor.

The yield spectra of the $[M+H]^{2+\bullet}$ ions (for LeuEnk represented by the corrected yield of the isotopic peak) reach their maxima at 16.5 eV and drop again until 21 eV. Furthermore, both spectra show some low yield in the energy range of 10.75 eV and below. However, since for both peptides the mass spectrum measured at 13 eV is the first one clearly featuring the isotopic peak of the $[M+H]^{2+\bullet}$ ion, we attribute all yield in the low energy regime to statistical noise. The yields measured for the photoionized LeuEnk precursor are ~30% higher than for MetEnk. Conclusively, the $[M+H]^{2+\bullet}$ ions of MetEnk are less stable, which is in line with the observation of the doubly charged fragments produced by neutral losses from the methionine side chain.

The spectra show that the vertical photoionization potentials of the two peptides must be between 10.75 and 13 eV. For singly protonated substance P (methionine containing peptide; 11 amino-acid residues) Canon et al. [5] measured an IE of 10.3±0.1 eV, which was 1.65 eV higher than the energy of the HOMO (8.7 eV; n_S orbital of the methionine side chain). This difference was considered to be an effect of Coulombic attraction between the positive charge of the proton and the departing electron. Adding this value to the assumed energies of the HOMOs of LeuEnk and MetEnk, 9.2 eV and 8.7 eV [23], respectively (see 3.1), results in an expected IE of ~10.85 for LeuEnk and 10.35 eV for MetEnk. Overall, the calculated IEs suggest that the actual IEs of the two peptides are closer to 10.75 eV than 13 eV, which is also roughly indicated by the trend of the left slope of feature C in the spectra of both peptides.

3.3.2 Singly charged species

Upon collision-induced dissociation the same fragments were detected for both peptides and the relative yields of all fragments were essentially identical (Fig. 2a). The only drastic difference was a ~4.5 times higher yield of y_1 (m/z 150) measured for MetEnk compared to the yield of the corresponding fragment of LeuEnk (m/z 132). A similar, yet weaker, trend has been reported before for the yields of the y_1 fragments of protonated Gly-Gly-Met and Gly-Gly-Leu and was explained by the higher proton affinity of the methionine residue [28].

In order to evaluate the effects of the methionine residue on the VUV photodissociation of MetEnk, the normalized yields of different detected immonium ions, side-chain fragments and backbone fragments of LeuEnk and MetEnk (see Fig. 8) are discussed in the following. The backbone fragments are mentioned in the order of their origin along the peptide, starting from the C-terminus.

Fragment M_{sc} (Fig. 8a) is mainly produced in the energy range of feature C. Additionally, the spectrum shows a weak peak centered at ~24 eV in the energy range of feature D, which is most likely attributed to excitations of inner valence electrons. The corresponding fragment of LeuEnk, L_{sc} (Fig. 8a) was not detected. The absence of L_{sc} could either mean that this fragment was not produced or that the low-mass cut-off of the trapping window was between m/z 65 and 75.

The immonium ions L_{im} and M_{im} (Fig. 8b) are produced at photon energies above 10 eV, with a maximum in the regime of feature C. The normalized yield of L_{im} is around 3.5 times higher than the yield of M_{im}. This difference can be explained by the fact that the dissociation channel leading to M_{im} is in competition with the production of M_{sc} and fragments involving neutral losses from the methionine side chain.

In the energy regimes of feature A and B, b_4 (Fig. 8c) is almost entirely absent for both LeuEnk and MetEnk. In contrast, significant yields of b_4 have previously been reported upon VUV photon-induced dissociation of gas-phase LeuEnk by Ranković et al. [17] at photon energies as low as 5.7 eV. The production of b_4 is the dissociation channel of LeuEnk with the lowest activation energy [16,29,30] and can, consequently, be induced by very low collision energies. Therefore, the reason for these opposing observations could be rooted in the differences between the trapping and collisional-cooling parameters. Lastly, it should be noted that in our experiment no significant yields of b_4 were observed in the precursor-only spectra as well.

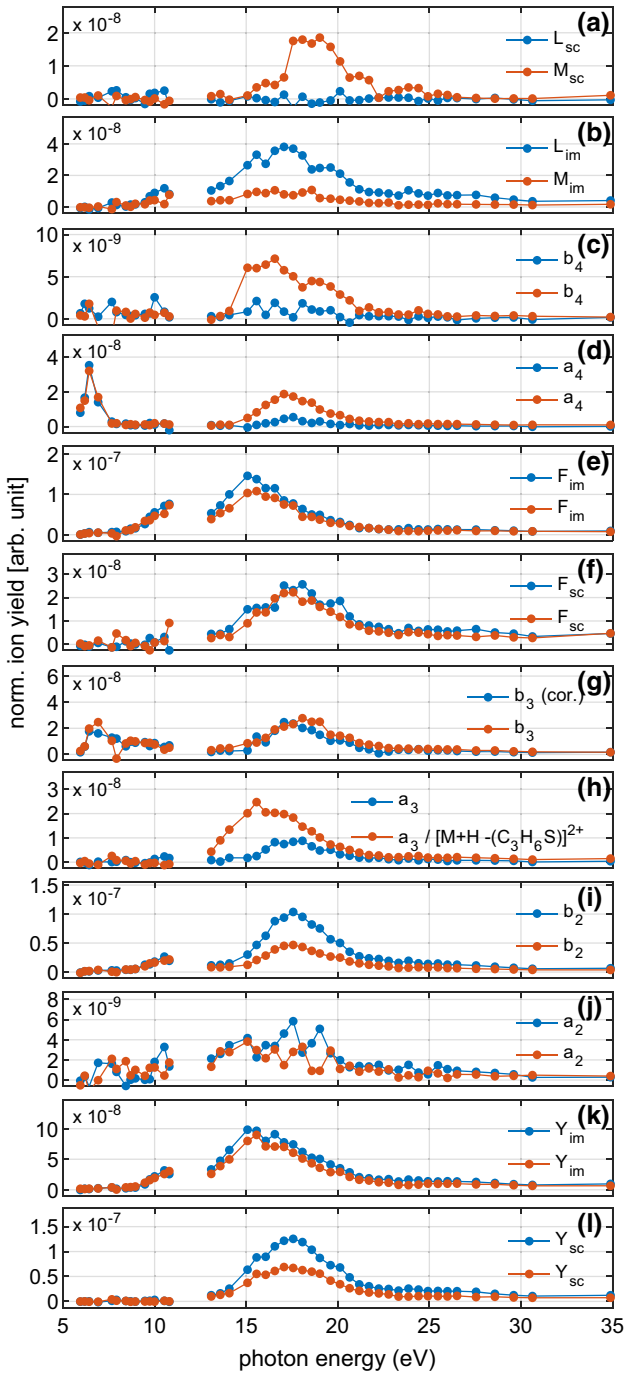

Fig. 8 Normalized yields of different immonium ions (im), side-cain fragments (sc) and backbone fragments measured upon VUV photon-induced dissociation of protonated LeuEnk (blue) and MetEnk (red)

Feature C in the normalized yield spectrum of the MetEnk b_4 fragment ranges from 15 to 21 eV. The respective spectrum for LeuEnk does not show any significant yield in this energy range. This means that upon photoionization there are dissociation channels of MetEnk where fragmentation takes place on the C-terminal side of the Phe-Met peptide bond (cleavage site of b_4), presumably within the methionine side chain, leaving the remaining system with enough internal energy for the production of the b_4 fragment. While upon photoexcitation at 7 eV the normalized yield of a_4 (Fig. 8d) is very similar for both peptides, in the regime of feature C the yield is four times higher for MetEnk than for LeuEnk. This effect supports the aforementioned idea that in MetEnk a first-step dissociation near the C-terminus produces fragments with enough internal energy to induce consecutive dissociation at the peptide bond between the phenylalanine and methionine residue. However, since the intensity of feature C measured for a_4 is higher than for b_4, it appears that either the cleavage of the C−CO bond is more favorable than the cleavage of the CO − NH bond in our experimental conditions or that, after dissociation, the internal energy of a_4 is significantly lower than the internal energy of b_4. In the latter case, b_4 would then be more likely to further dissociate, including the loss of CO to form the a_4 fragment, which is a well known dissociation pathway of b-type fragments under low-energy collision conditions [9].

In the 10 eV region the normalized yield of F_{im} (Fig. 8e) is almost identical for both peptides but at ∼15 eV it is slightly higher for LeuEnk than for MetEnk. Also the normalized yield of F_{sc} is very similar for both peptides (Fig. 8f). However, in contrast to F_{im}, F_{sc} is produced only in the energy regime of feature C and is not observed upon CID. This suggests that F_{sc} is mainly produced by radical-induced dissociation following photoionization. Interestingly, although the phenylalanine residue is next to the C-terminal leucine or methionine residue, the yields of F_{im} and F_{sc} are very similar between the two peptides. This could point towards the fact that these fragments are produced predominantly after photoabsorption in the phenylalanine side chain. Consequently, the dissociation process would not be influenced by the neighboring amino-acid residues.

The normalized yields of b_3 (Fig. 8g) are very similar for both peptides across the whole spectrum. In the case of LeuEnk the spectrum was corrected for the yield of the photoionized precursor ion (see 3.3.1). The high agreement between the spectra shows that the production of b_3 is not affected by the leucine or methionine residue. The normalized ion yield spectrum of the a_3 fragment of LeuEnk (Fig. 8h) shows a peak from 15 to 20 eV in the energy range of feature C. In the respective spectrum of MetEnk (Fig. 8h) this feature is more intense and begins already at 13 eV. In the case of MetEnk, most likely, the yields of the a_3 and $[M+H-C_3H_6S]^{2+\bullet}$ fragments are superimposed. When multiplying the spectrum of LeuEnk by 1.6 the right flanks of the peaks align. This indicates that for MetEnk the yield of a_3 is up to 60% higher than for LeuEnk. The idea that the left part of the peak is mainly due to the $[M+H-C_3H_6S]^{2+\bullet}$ fragment is supported by the fact that Canon et al. [5] reported an appearance energy of 12.3 eV for the corresponding fragment of the methionine-containing peptide substance P.

For both peptides the normalized yields of b_2 (Fig. 8i) are identical below 10 eV. The spectra of both peptides

feature a peak in the range of 15 to 22 eV. For LeuEnk this peak is twice as intense as for MetEnk. The ion yield spectra of a_2 (Fig. 8j) of both peptides (Fig. 8h) show some low yield at feature C. The values are, however, insignificant compared to the yields of the other a-type and b-type fragments.

The normalized yield of Y_{im} (Fig. 8k) is highly similar for both peptides. While this ion is produced at around 10 eV and in the regime of feature C, Y_{sc} (Fig. 8l) only occurs at feature C and is not observed upon CID. It can, therefore, be concluded that Y_{sc} is, like F_{sc}, produced by radical-induced dissociation following photoionization. The normalized yield of Y_{sc} is twice as high for LeuEnk than for MetEnk. Since the rate of photoionizations in the Tyr-Gly-Gly-Phe region of both peptides can be expected to be identical the decreased yield of Y_{sc} measured for MetEnk must be caused by an effect of the methionine residue. More precisely, it appears that the positive charge caused by photoionization of LeuEnk is more likely to migrate to the tyrosine residue where the radical-induced production of Y_{sc} is facilitated.

Overall, the VUV photon-induced dissociation of both peptides in the low energy region (6–10.75 eV) leads to very similar ion yields. At higher energies on the contrary, there are significant differences in the fragmentation behavior of the two systems. For MetEnk, higher normalized yields of a_4, b_4 and b_3 can be observed, while for LeuEnk the normalized yields of L_{im} (in comparison to M_{im}), b_2 and Y_{sc} are increased. These observations indicate that upon photoionization of MetEnk there is a high chance of the introduced positive charge moving towards the methionine residue where it facilitates localized fragmentation. After this initial step of fragmentation, the internal energy is localized at the dissociated bond. In a second step, the energy is directed towards the neighboring peptide bond between the phenylalanine and methionine residues which then cleaves, leading to the formation of b_4. In LeuEnk, on the contrary, the migration of the introduced charge does not seem to be affected by the leucine side chain and the dissociation channels are more distributed over the whole peptide.

In the post-ionization fragmentation pathways leading to b_4 the precursor ion must lose one positive charge and one or several complementary fragments with a combined mass of 149 u. A clear peak at *m/z* 88 was detected for MetEnk above the ionization threshold (see Fig. 4) that has not been reported for this peptide before. The loss of a charged fragment with a mass of 88 u from $[M+H - C_2H_5S^\bullet]^{2+}$ (*m/z* 256.5) would lead to b_4 (*m/z* 425). We, therefore, assign the peak at *m/z* 88 to a C-terminal fragment with sum formula $C_3H_6NO_2^+$ and propose the following dissociation pathway:

$$[M+H]^+ \xrightarrow{h\nu} [M+H]^{2+\bullet} + e^-$$
$$[M+H]^{2+\bullet} \xrightarrow{-C_2H_5S^\bullet} [M+H - C_2H_5S^\bullet]^{2+}$$
$$[M+H - C_2H_5S^\bullet]^{2+} \longrightarrow b_4^+ + C_3H_6NO_2^+$$

where, first, neutral loss of $C_2H_5S^\bullet$ (61 u) from the photoionized MetEnk precursor ion leads to $[M+H - C_2H_5S^\bullet]^{2+}$, which then dissociates into the positively charged fragments b_4 and $C_3H_6NO_2^+$. It is, however, likely that similar dissociation pathways like this exist, involving the formation of singly charged fragments with *m/z*-ratios below the mass cut-off of *m/z* 75, which would be an explanation for the difference between the measured total ion yields of the two peptides (see Sect. 3.1).

4 Conclusions

In order to investigate the extent of the effects of the methionine residue on the dissociation mechanism of small protonated peptides following valence shell photoexcitation and photoionization, we performed a VUV action spectroscopy study on gas-phase protonated LeuEnk and MetEnk covering the photon energy range of 6–35 eV.

In the (non-ionizing) photoexcitation regime, for both peptides the same fragments or pairs of corresponding fragments were detected and the measured ion yields were almost identical. Apart from low yields of fragments attributed to neutral side-chain losses, the observed fragmentation is highly similar to CID. One significant difference between the ion yields of the two peptides, however, is a higher yield of y_1 for MetEnk, which can be explained by the higher proton affinity of the methionine residue. The observations suggest that, on the whole, the electronic photoexcitation in this energy range is converted into vibrational energy. The internal energy is then efficiently redistributed over the peptide and is, eventually, followed by proton-directed fragmentation, unaffected by the methionine residue.

Upon photoionization, however, the obtained mass spectra showed significant differences. A comparison of different side-chain fragments, immonium ions and backbone fragments revealed that there are dissociation pathways in MetEnk involving an initial fragmentation step that takes place near the C-terminus. The hot intermediate fragments dissociate further, leading to the formation of the b_4 fragment. This is supported by the occurrence of several peaks attributed to neutral losses from the methionine side chain. In particular, one dissociation pathway was identified where, in a first step, $C_2H_5S^\bullet$ is split from the methionine side chain and then the remaining system dissociates into the b_4 and $C_3H_6NO_2^+$ fragment. The involvement of the methionine residue in this dissociation process clearly reflects the high electron hole affinity of this amino acid which efficiently directs the radical towards its side chain. More systematic studies with different positions of the methionine residue in the peptide and the influence of neighboring residues are planned to rationalize this effect.

Furthermore, the higher mass resolution of the present experiment in comparison to the past work on VUV photodissociation of LeuEnk [1,17] allowed for resolv-

ing the isotopic peaks of the photoionized precursor ions of both peptides. For LeuEnk this finally confirms undoubtedly that in the photoionization regime the peak measured at m/z 278 is to be attributed to both the intact photoionized precursor $[M+H]^{2+\bullet}$ and the b_3 fragment. While it was previously reported that such small peptides are not stable towards photoionization [7], our work revises the former threshold of ∼900 Da down to the size of the pentapeptides studied here. This strengthens the idea that VUV action spectroscopy can be particularly attractive for investigations of radical-driven processes in small singly protonated peptides for which standard electron transfer or electron capture dissociation techniques cannot be employed.

Acknowledgements We thank the Helmholtz-Center Berlin for the provision of synchrotron radiation at the U125-2_NIM beamline. S.Dörner, L.Schwob, K.Schubert and S.Bari acknowledge funding from the Helmholtz Initiative and Networking Fund through the Young Investigators Group Program (VH-NG-1104). Furthermore, K.Schubert, S.Techert and S.Bari were supported by the Deutsche Forschungsgemeinschaft, project B03 in the SFB 755 - Nanoscale Photonic Imaging. C.L.Pieterse was supported by the OrbiSIMS Project in the Life-Science and Health Programme of the National Measurement System of the U.K. Department of Business, Energy and Industrial Strategy (BEIS).

Funding Information Open Access funding enabled and organized by Projekt DEAL.

Data Availability Statement This manuscript has no associated data or the data will not be deposited. [Authors' comment: All relevant data generated during this study are contained in the published article.]

Conflict of interest There are no conflicts of interest to declare.

References

1. S. Bari, O. Gonzalez-Magaña, G. Reitsma, J. Werner, S. Schippers, R. Hoekstra, T. Schlathölter, J. Chem. Phys. **134**(2), 1 (2011). https://doi.org/10.1063/1.3515301
2. A.R. Milosavljević, C. Nicolas, J. Lemaire, C. Dehon, R. Thissen, J.M. Bizau, M. Réfrégiers, L. Nahon, A. Giuliani, Phys. Chem. Chem. Phys. **13**(34), 15432 (2011). https://doi.org/10.1039/c1cp21211g
3. A. Giuliani, A.R. Milosavljević, F. Canon, L. Nahon, M. Refregiers, J. Phys. Conf. Ser. **425**(12), 122001 (2013). https://doi.org/10.1088/1742-6596/425/12/122001
4. A. Giuliani, J.P. Williams, M.R. Green, Anal. Chem. **90**(12), 7176 (2018). https://doi.org/10.1021/acs.analchem.8b01789
5. F. Canon, A.R. Milosavljević, L. Nahon, A. Giuliani, Phys. Chem. Chem. Phys. **17**(17), 25725 (2015). https://doi.org/10.1039/c4cp04762a
6. A. Giuliani, A.R. Milosavljević, K. Hinsen, F. Canon, C. Nicolas, M. Réfrégiers, L. Nahon, Angew. Chem. Int. Ed. **51**(38), 9552 (2012). https://doi.org/10.1002/anie.201204435
7. O. González-Magaña, G. Reitsma, S. Bari, R. Hoekstra, T. Schlathölter, Phys. Chem. Chem. Phys. **14**(13), 4351 (2012). https://doi.org/10.1039/c2cp23470j
8. D. Egorov, R. Hoekstra, T. Schlathölter, Phys. Chem. Chem. Phys. **19**(31), 20608 (2017). https://doi.org/10.1039/C7CP03203J
9. B. Paizs, S. Suhai, Mass Spectrom. Rev. **24**(4), 508 (2005). https://doi.org/10.1002/mas.20024
10. L. Schwob, M. Lalande, D. Egorov, J. Rangama, R. Hoekstra, V. Vizcaino, T. Schlathölter, J.C. Poully, Phys. Chem. Chem. Phys. **19**, 22895 (2017). https://doi.org/10.1039/C7CP03376A
11. M. Abdelmouleh, M. Lalande, V. Vizcaino, T. Schlathölter, J.C. Poully, Chem. Eur. J. **26**(10), 2243 (2020). https://doi.org/10.1002/chem.201904786
12. F. Canon, A.R. Milosavljević, G. van der Rest, M. Réfrégiers, L. Nahon, P. Sarni-Manchado, V. Cheynier, A. Giuliani, Angew. Chem. Int. Ed. **52**(32), 8377 (2013). https://doi.org/10.1002/anie.201304046
13. W. Sun, H. Ren, Y. Tao, D. Xiao, X. Qin, L. Deng, M. Shao, J. Gao, X. Chen, J. Phys. Chem. C **119**(17), 9149 (2015). https://doi.org/10.1021/acs.jpcc.5b01740
14. X. Chen, Y. Tao, J. Li, H. Dai, W. Sun, X. Huang, Z. Wei, J. Phys. Chem. C **116**(37), 19682 (2012). https://doi.org/10.1021/jp306154x
15. M. Wang, J. Gao, P. Müller, B. Giese, Angew. Chem. Int. Ed. **48**(23), 4232 (2009). https://doi.org/10.1002/anie.200900827
16. J. Sztáray, A. Memboeuf, L. Drahos, K. Vékey, Mass Spectrom. Rev. **30**(2), 298 (2011). https://doi.org/10.1002/mas.20279
17. M.L. Ranković, F. Canon, L. Nahon, A. Giuliani, A.R. Milosavljević, J. Chem. Phys. **143**(24), 244311 (2015). https://doi.org/10.1063/1.4939080
18. A.R. Milosavljević, V.Z. Cerovski, M.L. Ranković, F. Canon, L. Nahon, A. Giuliani, Eur. Phys. J. D **68**(3), 68 (2014). https://doi.org/10.1140/epjd/e2014-40826-y
19. L. Schwob, S. Dörner, K. Atak, K. Schubert, M. Timm, C. Bülow, V. Zamudio-Bayer, B. von Issendorff, J.T. Lau, S. Techert, S. Bari, J. Phys. Chem. Lett.

11(4), 1215 (2020). https://doi.org/10.1021/acs.jpclett.0c00041
20. P. Baumgärtel, I. Packe, J. Large-scale Res. Facil. **2**, A53 (2016). https://doi.org/10.17815/jlsrf-2-76
21. G. Reichardt, J. Bahrdt, J.S. Schmidt, W. Gudat, A. Ehresmann, R. Müller-Albrecht, H. Molter, H. Schmoranzer, M. Martins, N. Schwentner, S. Sasaki, Nucl. Instrum. Methods Phys. Res. Sect. A Accel. Spectrom. Detectors Assoc. Equip. **467–468**, 462 (2001). https://doi.org/10.1016/S0168-9002(01)00359-X
22. D. Egorov, L. Schwob, M. Lalande, R. Hoekstra, T. Schlathölter, Phys. Chem. Chem. Phys. **18**(37), 26213 (2016). https://doi.org/10.1039/c6cp05254a
23. P.H. Cannington, N.S. Ham, J. Electron Spectrosc. Relat. Phenom. **15**(1), 79 (1979). https://doi.org/10.1016/0368-2048(79)87015-2
24. L. Serrano-Andrés, M.P. Fülscher, J. Am. Chem. Soc. **120**(42), 10912 (1998). https://doi.org/10.1021/ja981148+
25. A. Dawes, N. Pascual, S.V. Hoffmann, N.C. Jones, N.J. Mason, Phys. Chem. Chem. Phys. **19**(40), 27544 (2017). https://doi.org/10.1039/C7CP05319C
26. P. Roepstorff, J. Fohlman, Biol. Mass Spectrom. **11**(11), 601 (1984). https://doi.org/10.1002/bms.1200111109
27. R.W. Vachet, B.M. Bishop, B.W. Erickson, G.L. Glish, J. Am. Chem. Soc. **119**(24), 5481 (1997). https://doi.org/10.1021/ja9640758
28. D.G. Morgan, M.M. Bursey, Org. Mass Spectrom. **29**(7), 354 (1994). https://doi.org/10.1002/oms.1210290705
29. J. Laskin, J. Phys. Chem. A **110**(27), 8554 (2006). https://doi.org/10.1021/jp057229r
30. N.C. Polfer, B.C. Bohrer, M.D. Plasencia, B. Paizs, D.E. Clemmer, J. Phys. Chem. A **112**(6), 1286 (2008). https://doi.org/10.1021/jp0763937